Numerical Simulation of the Aerodynamic Loads acting on top of the SMART Centre for PV Applications

M. Raciti Castelli, S. Toniato, E. Benini

Abstract—The flow filed around a flatted-roof compound has been investigated by means of 2D and 3D numerical simulations. A constant wind velocity profile, based both on the maximum reference wind speed in the building site (peak gust speed worked out for a 50-year return period) and on the local roughness coefficient, has been simulated in order to determine the wind-induced loads on top of the roof. After determining the influence of the incoming wind directions on the induced roof loads, a 2D analysis of the most severe load condition has been performed, achieving a numerical quantification of the expected wind-induced forces on the PV panels on top of the roof.

Keywords—CFD, wind-induced loads, flow around buildings, photovoltaic system

I. INTRODUCTION

CURRENT trends in energy supply and use are patently unsustainable, as well as economically, environmentally and socially. Without decisive action, energy-related emissions of CO_2 will more than double by 2050 and increased oil demand will heighten concerns over the security of supplies [1]. Nevertheless, the rising concerns for the effects of the increased amount of greenhouse gases in the atmosphere have given solar photovoltaic (PV) industry a considerable push forward. Global PV capacity has in fact been increasing at an average annual growth rate of more than 40% since 2000 and it has significant potential for long-term growth over the next decades [1]. According to the last EPIA report, based on extensive analysis of five electricity markets (France, Germany, Italy, Spain and the United Kingdom), PV competitiveness with grid electricity can be achieved in some countries as early as 2013 and then spread across the continent in different market segments by 2020 [2].PV installations may be ground-mounted (and sometimes integrated with farming and grazing) or built into the roof or walls of a building, known as Building Integrated Photovoltaics (BIPV).

Marco Raciti Castelli is a Research Associate at the Department of Industrial Engineering of the University of Padova, Via Venezia 1, 35131 Padova, Italy and a fluid dynamic specialist at ESPE S.r.l., Via Cappello 12/A, 35010 San Pietro in Gu, Italy (phone: 0039-3207179239; e-mail: marco.raciticastelli@unipd.it).

Sergio Toniato is an Executive and Design Manager at ESPE S.r.l., Via Cappello 12/A, 35010 San Pietro in Gu, Italy (e-mail: stoniato@espe.it)

E. Benini is an Associate Professor at the Department of Industrial Engineering of the University of Padova, Via Venezia 1, 35131 Padova, Italy (e-mail: ernesto.benini@unipd.it).

In the last years, BIPV have increasingly been incorporated into the construction of new buildings as a principal or ancillary source of electrical power, although existing buildings may be retrofitted with BIPV modules as well [3]. However, as pointed out by Cosoiu et al. [4], the structure of the PV panel is rather flexible, continuous and fragile, sustained only by a thin framework: these features make it easily damageable by high winds and, in order to prevent such events, wind engineering experimental tests and numerical simulations are demanded if a more optimized and cheaper solution for a solar panel framework is required.

The complexity of the phenomena involved in the experimental investigation of the flow field around roof-mounted PV panels (and the consequent wind-induced loads on the supporting structures) gives an account of the use of computational fluid dynamics (CFD) aimed at determining the main structures of the flow field (recirculation bubbles, vertical air suction, vortices, three-dimensional effects), otherwise impossible to analyze. Several authors focused on the analysis of the flow field around buildings or bluff-shaped bodies [5] [6] [7].

Panneer Selvam [8] compared the computed pressure coefficients on the Texas Tech experimental building with experimental results, using both *k-ε* and *Kato-Launder k-ε* turbulence models and obtaining good agreement between numerical predictions and experimental measurements.

Calhoun et al. [9] compared the numerical prediction of a Reynolds-Averaged Navier Stokes (RANS) model with experimental measurements of the flow field around a complex building for several incoming wind directions, finding a good reproduction of the mean dynamics of the flow field and ascribing some numerical errors to the recirculation vortices that resulted shifted in space with respect to the experimental measured ones.

Baskaran and Kashef [10] applied CFD techniques for the prediction of wind flow conditions around a single building, between two parallel buildings and around a multiple building configuration. Finally, a case study was presented, simulating an existing site together with the existing building and the local landscape.

Yang et al. [11] conducted an experimental study to quantify the characteristics of flow structures and the resultant wind loads (both forces and moments) on a high-rise building model in tornado-like winds. A Particle Image Velocimetry

(PIV) system was also adopted to conduct detailed flow field measurements to reveal the evolution of the unsteady vortex and turbulent flow structures around the test model.

In order to develop a preliminary procedure to be used as a guidance in selecting the appropriate grid configuration and corresponding turbulence model for the prediction of the flow field over a two-dimensional roof architecture dominated by flow separation, Raciti Castelli et al. [12] tested the capability of several turbulence models to predict the separation that occurs in the upstream sector of the roof and the extension of the relative recirculation region for different vertical longitudinal positions, respectively from the upstream leading edge to the downstream bottom edge of a reference model building. Also spatial node distribution was investigated, in order to determine the best compromise between numerical prediction accuracy and computational effort. On the basis of this preliminary study, Raciti Castelli et al. [13] [14] numerically investigated the flow field over a 5° pitched roof-based integrated PV system, in order to determine the distribution of wind loads as a function of the panel row position on the roof and the amplitude of the recirculation region downstream the building. A solution for mitigating wind-induced loads on the panel rows was finally proposed, achieving a significant reduction of the resultant forces acting on the supporting frame of the PV panels.

Raciti Castelli and Benini [15] investigated the static pressure field on the top of a complex flat roof by means of a 3D numerical simulation of the flow field around the SMART shopping centre in Galliera Veneta (Italy). A constant wind velocity profile, based on both the maximum reference wind speed in the building site (peak gust speed worked out for a 50-year return period) and on the local roughness coefficient, was simulated, in order to determine the wind pressure loads acting on a roof-based PV system. A full campaign of numerical simulations allowed to analyze the effect of several wind directions on the static pressure field on the top of the roof. In the present work, the incoming wind direction (West-East) causing the most severe load condition on the top of the roof was examined through a 2D simulation of the flow field around a vertical section of the building, determining a numerical quantification of the aerodynamic forces acting on the supporting structure of the PV panels.

II. THE CASE STUDY AND PREVIOUS WORK

The SMART shopping centre of Galliera Veneta is located close to an industrial and commercial area placed on a wind plain in northern Italy. Figs. 1 and 2 show respectively a general aerial view of the geographical area and a close-up of the building site, while Figs. 3, 4 and 5 show some views of the building, also evidencing the vertical section examined in the presented numerical simulations.

A full campaign of 3D simulations was already performed in [15] by analyzing the effect of several incoming wind directions on the static loads acting on the top of the roof, thus determining the most severe wind-induced load condition on

the top of the roof as a function of the incoming wind sector. As can be seen from Fig. 6, most of the roof appeared to experience low static pressure: this phenomenon was ascribed to a large separation zone occurring on the top of the building, causing a wide recirculation bubble and consequent vertical air suction on the roof elements. Being the recirculation region connected with the severe impact of the velocity wind profile to the lateral walls of the building, the vertical air suction on top of the roof resulted maximized when the impact between the incoming flow and the lateral walls of the building was orthogonal (for North, South, West and East incoming wind directions). For more detail about the 3D simulation of the flow field around the SMART shopping centre, see [15].
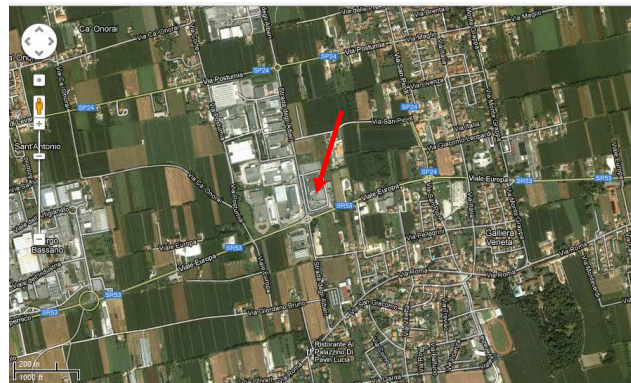

Fig. 1 Aerial view of the geographical area of the building site (evidenced by the red arrow)

Fig. 2 Aerial close-up of the building site (evidenced by the red perimeter); the parking areas, located north, south and west of the complex are evidenced by the orange arrows, while the vertical section examined in the 2D simulation is evidenced by the dashed yellow line

As can be seen from Fig. 7, representing the modulus of the negative static pressure peaks on top of the building as a function of the incoming wind direction, the most severe vertical air suction on the PV panels was caused by an incoming West-wind. The flow field around a West-East vertical section of the building was therefore investigated in the present work, thus demonstrating the feasibility of a simplified 2D analysis in order to reduce the computational

time (with respect to a much longer 3D simulation) and also to quantitatively investigate the distribution of aerodynamic forces along the top of the roof.

Fig. 3 South-West view of the building

Fig. 4 West view of the building; the vertical section examined in the 2D simulation is identified by the dashed yellow plane

Fig. 5 Displacement of the PV panels on the top of the SMART centre

III. DETERMINATION OF INLET WIND VELOCITY PROFILES

A constant wind velocity profile, based on the maximum reference wind speed in the building site (peak gust speed worked out for a 50-year return period) and on the local roughness coefficient, was simulated. After determining from [16] the values of $v_{b,0}$, a_0, c_t, k_r, z_0 and z_{min} for the building site, the reference wind speed was determined as:

$$v_b = v_{b,0} \tag{1}$$

being:

$$a_s \leq a_0 \tag{2}$$

and the coefficient of exposure for the building site was determined as:

$$c_e(H_{building}) = k_r^2 \, c_t \, \ln(H_{building}/z_0)[7 + c_t \, \ln(H_{building}/z_0)] \tag{3}$$

being:

$$H_{building} \geq z_{min} \tag{4}$$

The maximum reference wind speed for the building site was eventually determined as:

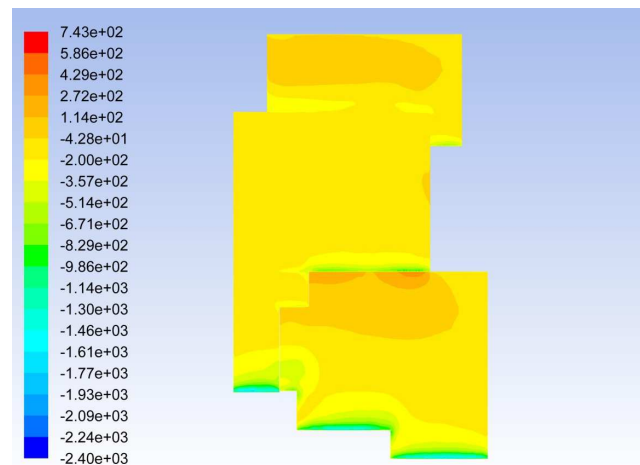$$v_{b,max} = [v_b^2 \, c_e(H_{building})]^{0.5} \tag{5}$$

Fig. 6 Static pressure distribution [Pa] on top of the SMART centre for an incoming South wind
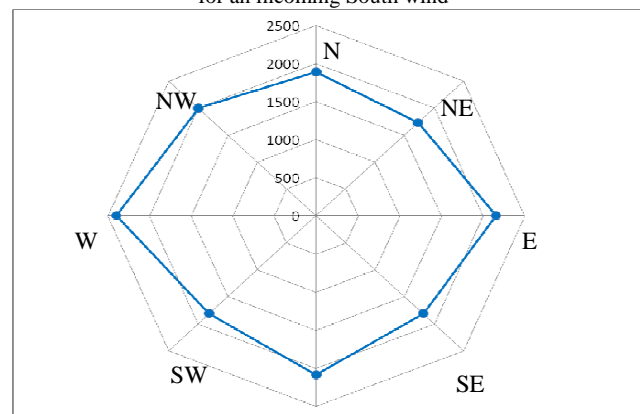

Fig. 7 Modulus of the negative static pressure peaks [Pa] on top of the SMART building as a function of the incoming wind direction

Table I summarizes the main coefficients adopted for the calculation of the maximum reference wind speed on the building site.

TABLE I
MAIN COEFFICIENTS ADOPTED FOR THE CALCULATION OF THE MAXIMUM REFERENCE WIND SPEED ON THE SMART BUILDING SITE, ACCORDING TO DM 14/01/2008 [16]

Denomination	Value
$v_{b,0}$ [m/s]	25
a_0 [m]	1000
a_s [m]	60
v_b [m/s]	25
c_t [-]	1
k_r [-]	0.22
z_0 [m]	0.30
z_{min} [m]	8
$H_{building}$ [m]	10.7 (max)
$c_e(H_{building})$ [-]	1.83
$v_{b,0}$ [m/s]	33.8

IV. MODEL GEOMETRY AND SPATIAL DOMAIN DISCRETIZATION

The flow field around the East-West vertical section of the SMART building was numerically simulated by reproducing a computational domain of rectangular shape, whose boundary conditions and main geometrical features are summarized in Fig. 8 and Table II.
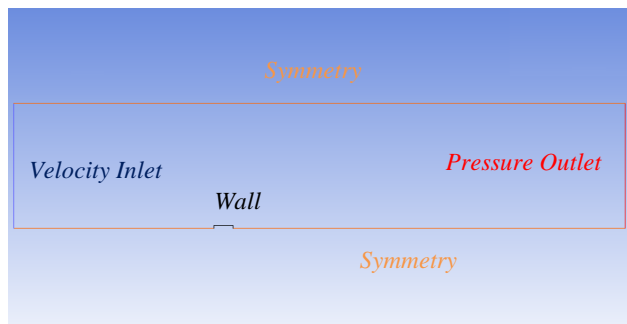

Fig. 8 Boundary conditions of the computational domain

TABLE II
MAIN DIMENSIONS OF THE COMPUTATIONAL DOMAIN

Denomination	Value [m]
Computational domain length	1930
Computational domain height	400
Distance from inlet boundary condition to the leading edge of the building	630

A symmetry boundary condition was adopted for the terrain, in order to avoid the development of an atmospheric boundary layer: this choice, though not realistic, allowed to invest the tested model with an uniform velocity profile, computed according to DM 14/01/2008 [16].

An isotropic unstructured mesh, whose resolution was based on the validation work performed by Raciti Castelli et al. [12],

was created around the model building. The characteristic data of the adopted grid architecture are summarized in Table III, as a function of the normalized grid resolution on the building, defined as:

$$Res_{building} = \Delta g_{building}/H_{building} \quad (6)$$

and as a function of the normalized grid resolution on outer computational domain, in formulas:

$$Res_{domain} = \Delta g_{domain}/H_{domain} \quad (7)$$

TABLE III
CHARACTERISTIC DATA OF THE ADOPTED SPATIAL DOMAIN DISCRETIZATION

Denomination	Value
$Res_{building}$ [-]	0.025
Growth factor [-]	1.1
Res_{domain} [-]	0.25

Figs. 9 and 10 show the main features of the spatial domain discretization. For further details upon the validation procedure and the reliability of the adopted numerical settings (as far as grid resolution and turbulence model are concerned), see [12].
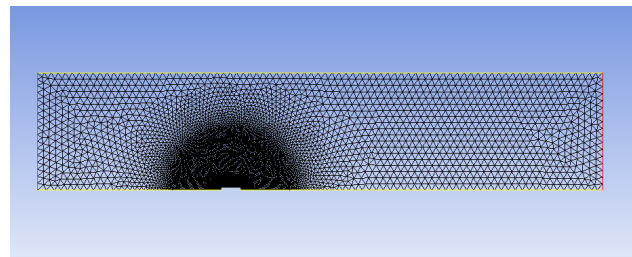

Fig. 9 Overall view of the spatial domain discretization of the computational domain
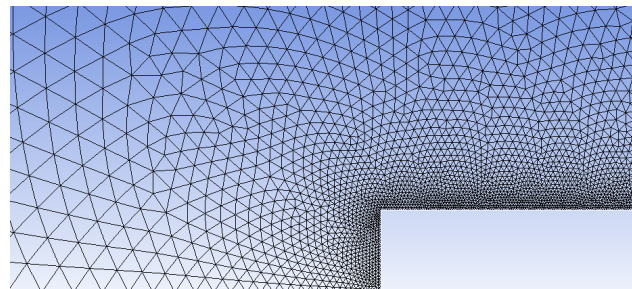

Fig. 10 Spatial domain discretization close to the building

V. TURBULENCE MODELS AND CONVERGENCE CRITERIA

The proposed numerical simulations were performed using the commercial code ANSYS FLUENT®, which implements 2D RANS equations using a finite volume based solver. Being the maximum velocities on the order of 70 m/s, the fluid was assumed to be incompressible, setting air density to 1.225 kg/m^3.

A segregated solver, implicit formulation, was chosen for steady flow computations. Standard k-ε model was used for turbulent calculations as suggested by Yoshie et al. [17].

As a global convergence criterion, residuals were set to 10^{-5}. Each simulation, performed on a 2.33 GHz clock frequency quad core CPU with Hyper-Threading, required a total computational time of about 2 hours.

VI. RESULTS AND DISCUSSION

Fig. 11 shows the contours of absolute velocity around the East-West vertical section of the building. A stagnation zone (evidenced by the red circle) is clearly visible on top of the roof, where the relative static pressure drops down to a negative value, as can be seen from Fig. 12, representing the static pressure contours around the building.
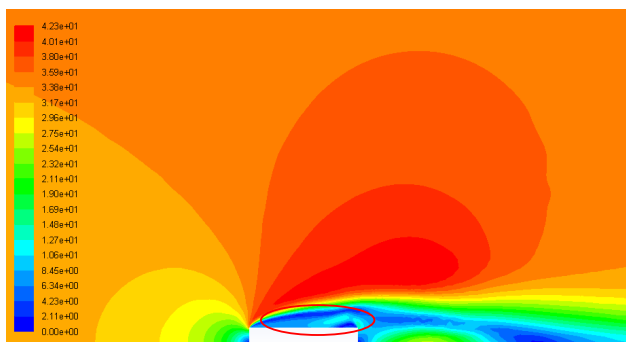

Fig. 11 Contours of absolute velocity [m/s] around the East-West vertical section of the SMART centre; the red circle evidences the stagnation zone on top of the roof
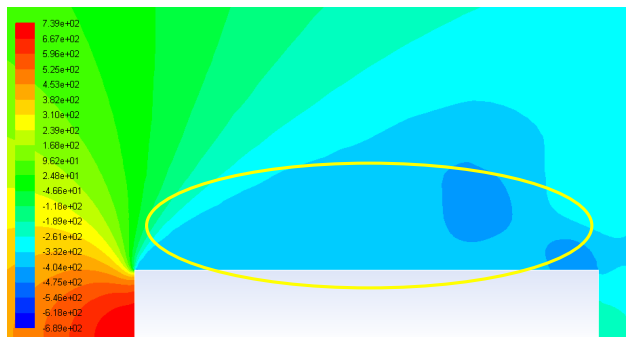

Fig. 12 Contours of static pressure [Pa] around the East-West vertical section of the SMART centre; the yellow circle evidences the negative relative pressure zone on top of the roof

The resulting separation bubble on top of the roof is clearly visible from Fig. 13, showing the absolute pathlines - colored by particle variables - around the building. In order to achieve a numerical quantification of the aerodynamic forces acting on the PV panels, the roof was subdivided into 63 horizontal sectors of 1 m length, numbered from 1 to 63 starting from the upstream edge of the building, as evidenced from Fig. 14.

Figs. from 15 to 17 show the horizontal, vertical and resultant forces per unit length on the roof of the building as a function of the roof sector number. As can be clearly seen, the horizontal forces on the roof are completely negligible, while no downward force is registered on the roof sectors. On the contrary, all sectors are subjected to upward thrusts, due to the low pressure in the recirculation zone on top of the building, as a consequence of the large separation bubble on top of the building.
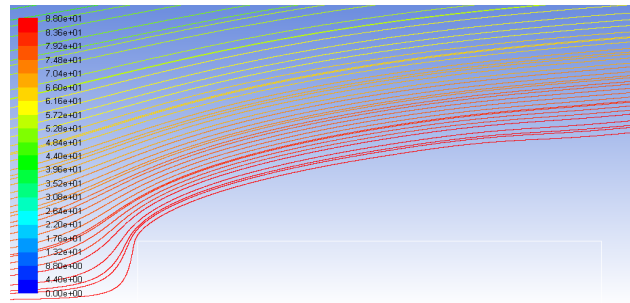

Fig. 13 Absolute pathlines colored by particle variables around the SMART building
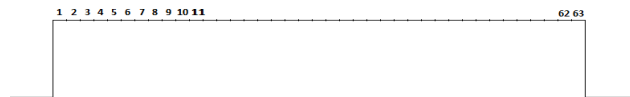

Fig. 14 Subdivision of the roof into 63 horizontal sectors, starting from the upstream edge of the building
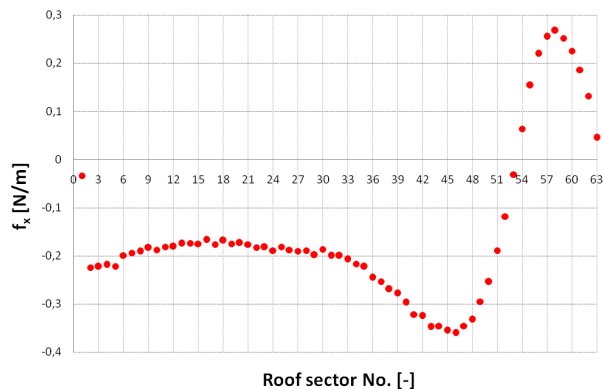

Fig. 15 Horizontal force per unit length on the examined roof sectors
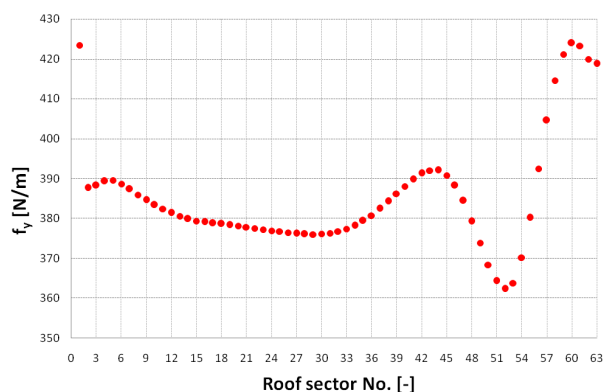

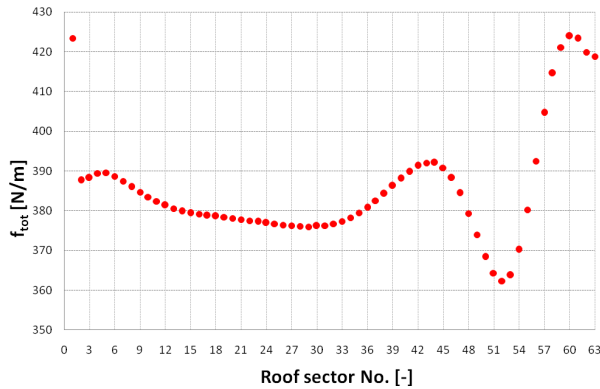Fig. 16 Vertical force per unit length on the examined roof sectors

Fig. 17 Resultant force per unit length on the examined roof sectors

VII. CONCLUSIONS AND FUTURE WORK

A two-dimensional numerical model for the evaluation of wind-induced loads on the top of a flat roof compound was presented. After determining the most severe load condition as a function of the incoming wind sector, a constant wind velocity profile, based on the maximum reference wind speed in the building site and on the local roughness coefficient, was simulated for an East-West vertical section of the building.

Owing to a large recirculation zone on top of the building, no downward force was registered on the horizontal roof. On the contrary, all roof sectors resulted subjected to a severe upward thrust.

Further work should be performed, in order to investigate a means for the vertical aerodynamic loads on the PV panels on top of the building by balancing the negative pressure field on both sides (upper and lower) of each panel.

NOMENCLATURE

a_0 [m]	reference height above sea level for the building site
a_s [m]	height of the building site above sea level
$c_e(H_{building})$ [-]	coefficient of exposure for the building site
c_t [-]	coefficient of topography for the building site and height
f_x [N/m]	horizontal force per unit length on the roof sector
f_y [N/m]	vertical force per unit length on the roof sector
f_{tot} [N/m]	total force per unit length on the roof sector
$H_{building}$ [m]	building height
k_r [-]	reference roughness coefficient at the building site
$Res_{building}$ [-]	normalized grid resolution on the building
Res_{domain} [-]	normalized grid resolution on outer computational domain
v_b [m/s]	basic wind speed at the building site and height above sea level
$v_{b,0}$ [m/s]	basic wind speed at the building site
$v_{b,max}$ [m/s]	maximum reference wind speed for the building site
z_0 [m]	reference height of roughness coefficient for the building site
z_{min} [m]	minimum reference height of roughness co-efficient for the building site
$\Delta g_{building}$ [m]	grid resolution on the building
Δg_{domain} [m]	grid resolution on outer computational domain

REFERENCES

[1] IEA (International Energy Agency), *Technology Roadmap – Solar photovoltaic energy*, 2010.
[2] EPIA (European Photovoltaic Industry Association), A. T. Kearney Strategic Consulting, *Solar Photovoltaics – Competing in the Energy Sector*, September 2011.
[3] P. Eiffert and G. J. Kiss, *Building-Integrated Photovoltaic Designs for Commercial and Institutional Structures: a Source Book for Architect*, U.S. Department of Energy (DOE), Office of Power Technologies, Photovoltaics Division, Federal Energy Management Program, 2000.
[4] B. Cosoiu, A. Damian and R. M. Damian, "Numerical and Experimental Investigation of Wind Induced Pressures on a Photovoltaic Solar Panel", *4th IASME/WSEAS International Conference on Energy, Environment, Ecosystems and Sustainable Developments (EEESD'08)*, Algrave (Portugal), June 11-13, 2008.
[5] J. P. Castro and M. Dianat, "Surface Flow Patterns on Rectangular Bodies in Thick Boundary Layers", *Journal of Wind Engineering and Industrial Aerodynamics*, Vol. 11, pp. 107-119, 1984.
[6] R. Martinuzzi and C. Tropea, "The Flow around Surface-Mounted, Prismatic Obstacles Placed in a Fully Developed Channel Flow", *ASME Journal of Fluids Engineering*, Vol. 115, pp. 85-92, 1993.
[7] E. R. Meinders, K. Hanjalic and R. Martinuzzi, "Experimental Study of the Local Convection Heat Transfer from a Wall-Mounted Cube in Turbulent Channel Flow", ASME Journal of Heat Transfer, Vol. 121, pp. 564, 573, 1999.
[8] R. Panneer Selvam, "Computation of flow around Texas Tech building using k-ε and Kato-Launder k-ε turbulence model", Engineering Structures, Vol. 18, No. 11, pp. 856-860, 1996.
[9] R. Calhoun, F. Gouveia, J. Shinn, S. Chan, D. Stevens, R. Lee and J. Leone, "Flow around a Complex Building: Comparisons between Experiments and a Reynolds-Averaged Navier Stokes Approach", *Journal of Applied Meteorology*, Vol. 43, No. 5, pp. 696-710, 2004.
[10] A. Baskaran and A. Kashef, "Investigation of air flow around buildings using computational fluid dynamics techniques", Engineering Structures, Vol. 18, No. 11, pp. 861-875, 1996.
[11] Z. Yang, S. Partha and H. Hu, "Flow around a High-Rise Building Model in Tornado-like Wind", 46th AIAA Aerospace Sciences Meeting and Exhibit, Orlando (Florida), Jan 5-8, 2008.
[12] M. Raciti Castelli, A. Castelli and E. Benini, "Modeling Strategy and Numerical Validation of the Turbulent Flow over a two-Dimensional Flat Roof", *World Academy of Science, Engineering and Technology*, Issue 79 (2011), pp. 461-467.
[13] M. Raciti Castelli, S. Toniato and E. Benini, "Numerical Analysis of Wind Induced Pressure Loads on an Integrated Roof-Based Photovoltaic System", *MAS 2011, 10th International Conference on Modeling and Applied Simulation*, Rome (Italy), 12-14 September, 2011.
[14] M. Raciti Castelli, S. Toniato and E. Benini, "Mitigation of Wind Induced Pressure Loads on an Integrated Roof-Based Photovoltaic System through 2D Numerical Simulation", *CSSim 2011 International Conference on Computer Modelling and Simulation*, Brno (Czech Republic), 5-7 September, 2011.
[15] M. Raciti Castelli, S. Toniato, E. Benini, "Numerical Simulation of Wind-Induced Pressure Loads on a Flat Roof Building", *e-Nova 2011, Sustainable Buildings – Cutting Edge Technologies & Concepts for Future Buildings*, Campus Pinkafeld (Austria), 24-25 November, 2011.
[16] DM 14/01/2008 – *Norme tecniche per le costruzioni*, issued on the Italian Gazzetta Ufficiale on February 4, 2008.
[17] R. Yoshie, A. Mochida, Y. Tominaga, H. Kataoka, T. Harimoto, T. Nozu, T. Shirasawa, "Cooperative project for CFD prediction of pedestrian wind environment in the Architectural Institute of Japan", *Journal of Wind Engineering and Industrial Aerodynamics*, Vol. 95 (2007), pp. 1551-1578.